Operational Techniques for Determining SWE by Sound Propagation through Snow: I. General Theory

NICHOLAS J. KINAR[43] AND JOHN W. POMEROY[1]

ABSTRACT

Recent research has demonstrated that an acoustic pressure wave can be used to determine Snow Water Equivalent (SWE) without the need for gravimetric sampling. The application of this technique poses a number of challenges in cold environments due to the presence of snow with wind crusts, ice layers, buried vegetation, high liquid water content and due to the extensive signal processing required after collection of returned sound waves. A new automated procedure for determining SWE by an acoustic wave has been developed. This paper presents the theory of the new procedure and discusses the selection of parameters required for the operational realization of an acoustic sampling system. Images of a rough snow interface were analyzed using fractal techniques. The image analysis procedure showed that rough snow interfaces can be modeled as fractal Brownian motion (fBm) processes. A fractal model of the rough snow interface was used to calculate the acoustic scattering of an incident sound wave. Recursive relationships were used to predict the footprint area of the acoustic wave on successive snow interfaces. An analysis of the high frequency assumption used to calculate the phase velocity of the sound pressure wave in the snowpack is also presented.

INTRODUCTION

Accurate assessment of water availability from snowmelt is crucial in regions where demand for water consumption exceeds the water available for use and in regions subject to snowmelt flooding. SWE has been used to determine the maximum amount of water that is potentially available as agricultural runoff during the time of ablation. Measurements of SWE can also help to validate and provide inputs for atmospheric and hydrological models with respect to their accuracy over cold regions (Pomeroy *et al.*, 2007).

Procedures used to determine SWE often involve the use of instrumentation that is time-consuming to operate, expensive to deploy, and prone to instrument and human error. Devices which have been used in the measurement of SWE include gravimetric snow samplers; snow pillows; Frequency-Modulated Continuous-Wave (FMCW) radar systems; and gamma-ray attenuation and passive microwave radiation sensors (Pomeroy and Gray, 1995).

In a recent paper, a technique was presented for determining SWE by an acoustic impulse (Kinar and Pomeroy, 2007). Two sonic wave transducers were positioned above the snow surface. One of the transducers was used to send a sound wave into the snowpack. Reflections of the sound wave from the snow were detected by the other transducer and signal processing techniques were utilized to estimate SWE.

The acoustic SWE technique has a number of advantages over other SWE measurement techniques. One advantage is that the use of an acoustic wave permits non-invasive measurement of SWE. This allows for SWE measurements to be made without physically disrupting the snowpack. Changes in SWE at one

[43] Centre for Hydrology, University of Saskatchewan, 117 Science Place, Saskatoon, Saskatchewan, S7N 5C8 Canada

location can be tracked without the need for instrumentation to be permanently installed under the snow surface. Acoustic snow surveys are logistically easier because gravimetric snow samples do not have to be extracted. Unlike radar devices, which rely on the use of high-current sourcing power supplies and large antennas to produce and receive electromagnetic waves, small and portable acoustic transducers can be powered by inexpensive electronic circuits with modest power requirements.

However, one disadvantage of the Kinar and Pomeroy (2007) acoustic technique was that signal processing of the sound wave reflected from the snowpack could not be performed in real-time. In a similar fashion to seismic interpretation, the signal processing generated information from the sound wave that must be examined by a human operator before SWE was calculated. This precluded the automated determination of SWE. The implications are that acoustic sampling of SWE could not be efficiently performed at the same time scale as other measurements taken at a meteorological station due to the large amounts of data that must be interpreted. Moreover, use of this acoustic technique for snow surveying did not permit the surveyor to immediately determine whether the acoustic measurement was successful.

This paper describes how the acoustic technique has been recently improved so that it can be used in an operational context. This permits the signal processing to be conducted in the field using custom electronic circuits that are portable and easily transported to remote locations. The device constructed for signal processing allows for repeatable measurements of SWE to be made using an acoustic wave. These measurements contribute to observations made by other investigators in snow acoustics and help to establish observational techniques for further research into the physical properties of snow.

THEORY

Snowpack model

A downward-facing transducer T_s situated at a distance y_0 (m) above the surface Ω_0 of the snowpack produces a sound pressure wave p_0^+ (Figure 1). The sound wave has a bandwidth $B = f_1 - f_0$ situated between two frequencies, f_0 (Hz) and f_1 (Hz), where $f_1 > f_0$. Because the frequencies are in the audible sound range (~20 Hz to ~20 kHz), the transducer T_s is a moving-armature (magnetic coil) loudspeaker. The sound pressure wave is transferred to the pore spaces of the snowpack by acoustic-to-seismic coupling (Albert, 2001; Albert, 1993a; Albert, 1993b; Albert, 1987; Albert and Orcutt, 1990; Albert and Orcutt, 1989). The transducer is situated at a point coincident with a line that is at an angle of incidence θ_0 (radians) close to the normal, such that $\theta_0 \to 0$. This is more realistic than assuming that $\theta_0 = 0$ since if the transducer is fastened on an instrument held in the hand of a snow surveyor, variations in θ_0 can be caused by human error and wind effects. The sound wave produced by the transducer also travels directly in the air as p_c toward another downward-facing transducer T_R which is situated at a distance of x_d (meters) from T_s. This second transducer is a microphone which receives reflections of the sound pressure wave p_0^- from the snowpack, but will also detect the air-coupled direct wave. Because the frequencies produced by T_s are in the audible range, the transducer T_R is selected to be an electret microphone with a generally flat frequency response.

The snowpack is comprised of layers $\{L_1, \ldots, L_N\}$ demarcated by interfaces $\{\Omega_0, \ldots, \Omega_N\}$ corresponding to changes in acoustic impedance. The total number of snow layers is N. The first layer L_0 is the air layer situated above the surface of the snowpack, which has an average gas density of $\overline{\rho}_0$ (kg m^{-3}), and the first interface Ω_0 is the air-snow interface. It is possible that the layers in the snowpack are produced by wind crusts, snow deposition events, or ice from rain-on-snow events. The layers are defined due to changes in acoustic properties causing a reflection of the wave. Scattering is considered in two dimensions only for this model.

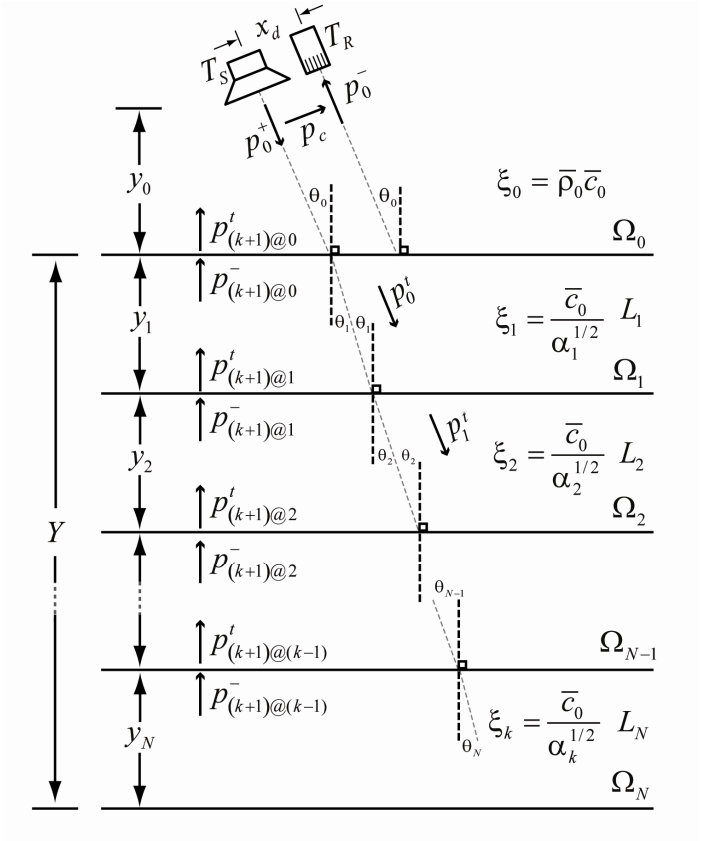

Figure 1. Diagram of the snowpack model. Nomenclature for this diagram is discussed in the text. The nomenclature for the pressure-tracking algorithm $\left\{p^-_{(k+1)@(k-1)}, p^t_{(k+1)@(k-1)}\right\}$ is discussed by Kinar and Pomeroy (2008).

The average phase velocity of the wave in the pore spaces of the layer L_k is taken to be $\overline{c}_k$ (m s^{-1}). Although the phase velocity may change with depth in the snow due to compaction and metamorphic processes, it is not possible to predict this change because the snowpack is considered as a black-box system where the reflections are used to predict the snow physical properties in a discrete fashion at a particular depth beneath the snow surface.

Each layer L_k is assumed to be a porous material which is comprised of a partially air-saturated ice framework with pore spaces characterized by porosity ϕ_k and tortuosity α_k. The porosity ϕ_k (dimensionless) is defined as the fraction of pore spaces in the snow (Jones *et al.*, 1999), whereas the tortuosity α_k (dimensionless) is defined as the straight-line deviation through the pore spaces of the medium. The tortuosity can be calculated as the ratio of the pore length distance to the straight line distance between the endpoints of the pore distance (Suman and Ruth, 1993). The tortuosity of a porous substance is always greater than unity ($\alpha > 1$) because a straight line is the shortest distance between two points. Higher values of the tortuosity are indicative of pore spaces with a greater proportion of twists and turns. Tortuosity can be directly measured using tomographic (Coléou *et al.*, 2001; Kaempfer *et al.*, 2005; Kerbrat *et al.*, 2008) or Magnetic Resonance Imaging (MRI) techniques (Wang *et al.*, 2005).

As predicted by the Biot theory of sound propagation through porous media (Biot, 1956a; Biot, 1956b), the sound pressure wave propagates through the snowpack (Johnson, 1982) as two types of pressure wave (P_1-wave and P_2-wave) and one type of shear wave (S-wave). The P_1-wave travels through the ice framework of the snow, whereas the P_2-wave propagates through the pore spaces. The S-wave propagates through the ice structure. There is coupled motion between the three types of waves. The phase velocity and attenuation of the P_2-wave is dependent on the source frequency. Less attenuation of the P_2-wave will be observed for lower sound frequencies (Albert, 1993a).

In this model, we are concerned with the P_2-wave propagating through the pore spaces of the snow due to the stiffness of the frame relative to the air saturating the pore spaces (Albert, 1993b). Because the air

above the snowpack is a gas, and is therefore incapable of shear, the reflections of the P_2-wave due to changes in the acoustic impedance of the layers will be detected as pressure fluctuations by the microphone at small angles of incidence to the surface normal.

Snowpack interfaces

An interface Ω_k in the snowpack can be represented as a plane curve, which is the best-fit straight line through undulations in the boundary caused by variations in the snowpack owing to wind redistribution of snow, topography, and the influence of vegetation on snow deposition (Kinar and Pomeroy, 2007). In the absence of any information on the roughness of the snow surface, Ω_k can be modeled using fractal techniques to examine the influence of acoustic scattering of the incident sound wave by the interface.

Broadly defined, a fractal is a geometric construct which has the property of self-similarity at various scales. Mathematical fractals such as the Koch snowflake (Lapidus and Pang, 1995) or the Julia set (Shishikura, 1998) preserve the self-similarity property over all spatial scales, whereas statistical fractals have self-similarity over only a limited number of scales (Falconer, 1990). Fractals are mathematical constructs with a non-integer dimension D referred to as the Hausdorff–Besicovitch dimension (Alberverio *et al.*, 2004). Fractals can be classified as having only one dimension, "monofractals," or as having multiple dimensions, "multi-fractals" (Sornette, 2006). The properties of fractals make these constructs ideal for modeling a variety of physical elements including river morphology (Claps *et al.*, 1996), snow interception and sublimation (Pomeroy and Schmidt, 1993), snow ablation (Shook and Gray, 1997; Shook *et al.*, 1993), groundwater flow processes (Vogel and Roth, 2003), and natural landscapes (Tyre *et al.*, 1998).

A fractal surface for modeling acoustic scattering processes for reflection at a rough interface can be approximated by a discrete form of the band-limited Weierstrass–Mandelbrot function (Cai *et al.*, 2006; Summers *et al.*, 2005). To calculate the rough snow interface for a set of discrete points $\{x_0,\ldots,x_N\}$, we recursively define a version of this function as:

$$g[x_0] = \sum_{m=0}^{M} (D-1)^m \sin\left(\kappa b_f^m x_0 + \beta_m\right) \tag{1}$$

$$f[x_0] = \Delta y_{\mathrm{RMS}} C g[x_0] \tag{2}$$

$$\Delta y_{\mathrm{RMS}} = \left(\frac{1}{N}\sum_{i=0}^{N-1} y_i^2\right)^{1/2} \tag{3}$$

$$C = \left[\frac{2D(2-D)}{1-(D-1)^{2M}}\right]^{1/2} \tag{4}$$

$$\kappa = \frac{2\pi}{\Lambda} \tag{5}$$

where Δy_{RMS} (dimensionless) is the Root-Mean-Squared (RMS) displacement of the interface from a reference level $f[x]=0$, C is an amplitude parameter, D has been proven to be the Hausdorff–Besicovitch dimension (Szulga, 2002), M is the total number of harmonic components, κ is the spatial wave number (m^{-1}), Λ is the spatial period of displacements in the vertical height of the interface, b_f is a frequency-scaling parameter, and β_m is the phase-shift (radians) at a given harmonic frequency component m.

Surface roughness

The surface roughness of Ω_k is modeled using the slope angles of the fractal curve generated from evaluation of Equation (2). This ensures that the surface is described by the V-cavity paradigm (Torrance and Sparrow, 1967) which is widely used to model diffuse reflections from rough surfaces. The surface roughness over the extent of the curve in two dimensions is assumed to be the same as the surface roughness in three dimensions.

The sequence θ_s of surface slope angles is calculated by:

$$\theta_s = \arctan\left(\nabla f\left[x\right]\right) \tag{6}$$

where $\nabla = \left(\partial / \partial x\right)\hat{\mathbf{i}}$, and the inverse tangent (arctangent) is being calculated for each element in the $\nabla f\left[x\right]$ sequence to generate the sequence θ_s.

The standard sample deviation σ_r (rad) of the total number of slope angles N_x is used to measure the generated surface roughness (Lurton, 2002):

$$\sigma_r = \left[\frac{1}{N_x - 1}\sum_{i=1}^{N_x}\left(\theta_{s,i} - \bar{\theta}_s\right)\right]^{1/2} \tag{7}$$

where $\bar{\theta}_s$ (radians) is the mean value of the calculated sequence of slope angles, and $\theta_{s,k}$ refers to a particular slope angle $k \in \theta_s$.

The dimensionless Rayleigh parameter $P_{R,(\Omega,k)}$ from wave scattering theory is used to quantify the vertical surface roughness (Brekhovskikh and Lysanov, 2003). Because the incident sound pressure wave has a bandwidth between f_0 and f_1, the Rayleigh parameter is frequency integrated:

$$\begin{aligned} P_{R,(\Omega,k)} &= \frac{1}{f_1 - f_0}\int_{f_0}^{f_1}\frac{4\pi\bar{c}_k\sigma}{f}\cos\left(\theta_k\right)df \\ &= \frac{4\pi\bar{c}_k\sigma\cos\left(\theta_k\right)}{f_1 - f_0}\left\{\ln\left(f_1\right) - \ln\left(f_0\right)\right\} \end{aligned} \tag{8}$$

where $\bar{c}_k$ (m s^{-1}) is the average phase velocity of the P_2 wave travelling in layer L_k.

Acoustic footprint

In radar or sonar applications the area on the snow surface contacted by the sound pressure wave from the transducer T_s is referred to as the "footprint" (Arcone *et al.*, 1997) or "insonified area" (Lurton, 2002) of the incident beam. The same terminology is used to describe the area on the snow surface contacted by the sound pressure wave from the loudspeaker.

Assuming that the transducer has an aperture angle of φ radians and that the transducer radiates the sound wave evenly over the aperture angle in the half-space above the snow interface, then at an angle of incidence of $\theta_0 \approx 0$ radians, the diameter $d_{f,0}$ (m) and area Φ_0 (m^2) of the beam footprint on the first air-snow interface is calculated as (Figure 2):

$$d_{f,0} = 2y_0\tan\left(\varphi/2\right) \tag{9}$$

$$\Phi_0 = \left(\pi/4\right)d_{f.0}^2 \tag{10}$$

where y_0 is the distance from the loudspeaker to the snow surface.

If the transducer is situated at an angle of incidence $\theta_0 > 0$ to the snow surface, the diameter and area of the footprint on the first air-snow interface becomes (Figure 2):

$$d_{f,0}^* = y_0\left\{\tan\left(\theta_0 + \frac{\varphi}{2}\right) - \tan\left(\theta_0 - \frac{\varphi}{2}\right)\right\} \tag{11}$$

$$\Phi_0^* = \pi d_{f,0}d_{f,0}^* \tag{12}$$

The diameter of the footprint projected by the incident sound wave on an interface Ω_k beneath the air-snow interface is calculated by finding the angles at which the base of the beam contacts the snow surface, and then recursively tracking the change in the footprint diameter throughout each of the snow layers.

When the sending and receiving transducers are situated at an angle of incidence of $\theta_0 = 0$ to the snow surface, the angles of incidence ϑ_k (radians) for the rays at the base of the beam are $\vartheta_{0,A} = \vartheta_{0,B} = \varphi/2$, or $\vartheta_{k,A} = \vartheta_{k,B}$ for successive interfaces Ω_k with $k \geq 1$. The angles of the transmitted rays are $\vartheta_{k+1,A}$ and $\vartheta_{k+1,B}$, and are determined. The footprint diameter and area on each of the layers in the snowpack are recursively calculated:

$$d_{f,k+1} = d_{f,k} + 2y_{k+1}\tan\left(\vartheta_{k+1}\right) \tag{13}$$

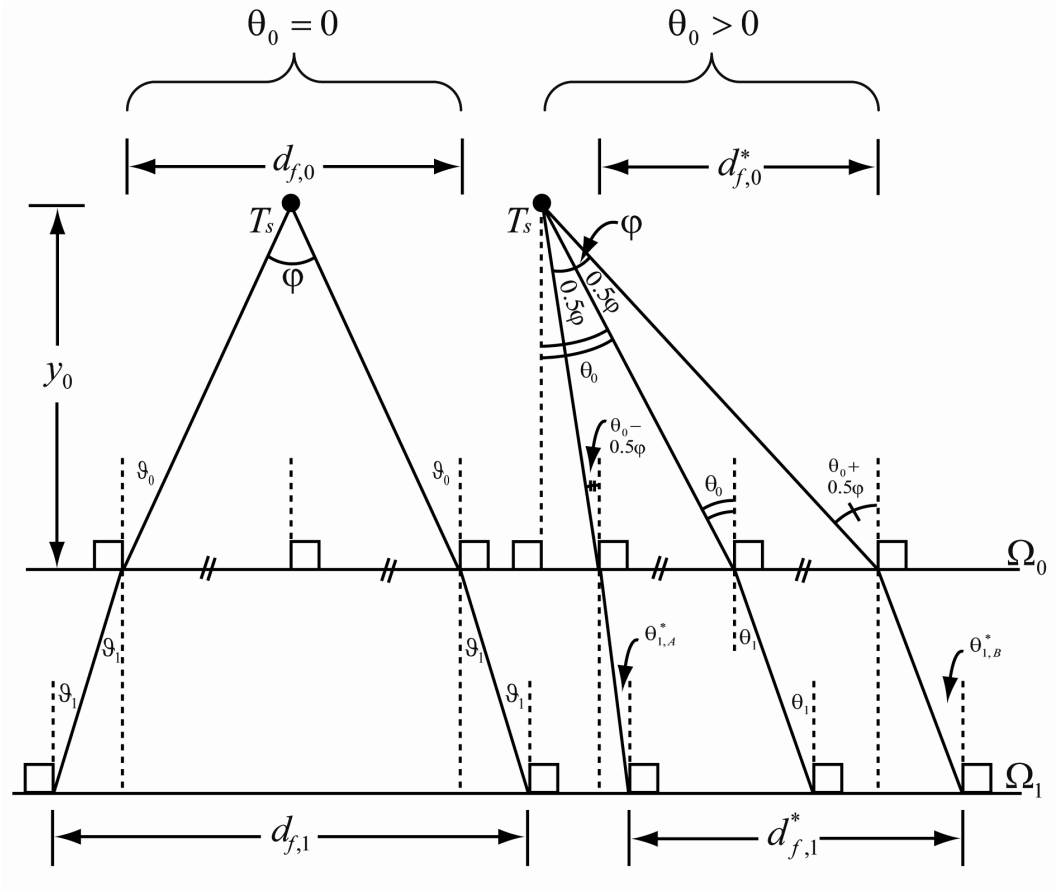

Figure 2. Diagram of the acoustic footprint on the first two snowpack layers. The nomenclature is discussed in the text.

$$\Phi_{k+1} = \left(\pi/4\right)d_{f,k+1}^2 \tag{14}$$

Alternately, when the sending and receiving transducers are tilted at an angle of incidence θ_0 to the snow surface, Equation (13) can be written using two angles of incidence expressible as the set $\left\{\theta_{k,A}, \theta_{k,B}\right\}$. The angles $\theta_{k,A}^*$ and $\theta_{k,B}^*$ are then independently tracked through each of the interfaces.

$$\vartheta_{0,A}^* = \theta_0 - \frac{\varphi}{2} \tag{15}$$

$$\vartheta_{0,B}^* = \theta_0 + \frac{\varphi}{2} \tag{16}$$

$$d_{f,k+1}^* = d_{f,k}^* + y_{k+1}\left\{\tan\left(\vartheta_{k+1,B}^*\right) - \tan\left(\vartheta_{k+1,A}^*\right)\right\} \tag{17}$$

$$\Phi^*_{k+1} = \pi d_{f,k+1} d^*_{f,k+1} \tag{18}$$

Phase velocity of the sound pressure wave

The compressibility of the air in the pore spaces of the snowpack is considered to be orders of magnitude greater than the compressibility of the frame comprised of snow particles (Albert, 2001). This allows for the average phase velocity $\overline{c}_k$ (m s^{-1}) of the sound pressure wave in the porous snow medium to be calculated as (Johnson and Plona, 1982; Johnson *et al.*, 1982):

$$\overline{c}_k = \frac{\overline{c}_0}{\alpha_k^{1/2}}, \qquad \text{for } \omega > \tilde{\omega} = \frac{2\eta_0}{\rho_0 a^2} \tag{19}$$

where η_0 (Pa s) is the dynamic viscosity of air in the pore spaces of snow, $\overline{\rho}_0$ (kg m^{-3}) is the average air density, and a is the mean diameter (meters) of the pore spaces in the snow porous medium. Equation (19) holds for $\omega > \tilde{\omega}$, where $\omega = 2\pi f$ is the angular frequency of the source, and $\tilde{\omega}$ (radians) is the threshold frequency, when f is given in Hertz.

Relationship between porosity and tortuosity

A relationship between the tortuosity and the porosity of porous materials has been identified from Biot theory (Berryman, 1980; Berryman, 1983) This relationship is dependent on a dimensionless shape factor γ determined from the geometry of the particles that comprise the medium:

$$\alpha_k = 1 - \gamma\left(1 - \frac{1}{\phi_k}\right) \tag{20}$$

The shape factor γ ranges between $0.5 \le \gamma \le 0.67$ for particles that can be approximated as perfectly spherical (0.5) or needle-shaped (0.67) (Berryman, 1980; Berryman, 1983; Johnson and Sen, 1981). Previous research has suggested that the Berryman relationship can be used to model the relationship between the porosity and tortuosity of snow (Kinar and Pomeroy, 2007).

Calculating snow water equivalent

The snow density $\overline{\rho}_k$ (kg m^{-3}) of the layer is determined from a well-known relationship often used in gravimetric sampling:

$$\overline{\rho}_k = \rho_{\text{ice}}\left(1 - \phi_k\right) \tag{21}$$

where $\rho_{\text{ice}} = 917$ kg m^{-3} is the density of ice.

The total snow depth Y (m) is recursively determined using the sum of the vertical dimension $y_k = \overline{c}_k t_k$ calculated for each of the layers L_k, where t_k (seconds) is the one-way travel time taken for the sound wave to propagate through a layer. The SWE (mm or kg m^{-2}) is then calculated by the relationship (Pomeroy and Gray, 1995):

$$\text{SWE} = \frac{Y}{N}\sum_{i=0}^{N} \rho_k \tag{22}$$

where $\{\rho_0, \ldots, \rho_N\}$ are the densities of the acoustic layers $\{L_0, \ldots, L_N\}$.

SIGNAL PROCESSING

Specialized signal processing is used to determine the porosity ϕ_k and the phase velocity $\overline{c}_k$ of the sound pressure wave in the snowpack (Kinar and Pomeroy, 2008). The sound wave sent from the loudspeaker is a Maximum Length Sequence (MLS), which is used to determine the impulse response of the layered snow medium (Borish and Angell, 1983; Rife and Vanderkooy, 1989). The MLS sequence ensures that a number of frequencies over the bandwidth B of the loudspeaker propagate through the snowpack. Because the MLS is a wideband signal, it is possible that there are frequencies of the sound wave less than the threshold frequency $\tilde{\omega}$ which travel in the pore spaces of the snowpack.

Reflections from the layers in the snowpack due to changes in acoustic impedance are detected by the microphone. The digitized reflection signal is then processed by an inversion algorithm (Kinar and Pomeroy, 2008) to determine the porosity ϕ_k. The inversion algorithm is able to obtain the attenuation coefficient ψ_k (m^{-1}) for a layer L_k. Because snow is a medium which strongly attenuates the P_2-wave, the attenuation coefficient can be used to calculate the reduction of sound pressure as the sound pressure wave propagates through the snowpack.

Inputs to this inversion algorithm are the area Φ_k of the acoustic footprint on a layer L_k and the Rayleigh parameter $P_{R,(\Omega,k)}$, which are calculated using the procedure outlined in the previous sections. The generated rough snow interface is used in this calculation to reduce the effects of acoustic scattering due to ice layers and vegetation. The average density $\overline{\rho}_k$ of the layer is then calculated by Equation (21). Equation (20) is then used to calculate the tortuosity α_k. Once the phase velocity $\overline{c}_0$ of the sound pressure wave in the air medium has been determined from an estimate of the air temperature T, the phase velocity $\overline{c}_k$ of the sound pressure wave in layer L_k is used to determine the travel time t_k of the wave in the layer and the vertical dimension y_k of the layer.

Recursive application of the inversion procedure allows for the total snow depth Y to be determined. Since the snow depth and the densities of each layer can be determined, the SWE is calculated by Equation (22). Because the reflections from the layers are determined by a peak detector, an estimate must be made of the snow depth using a ruler. This estimate is then used to suggest a maximum cut-off depth for the peak detector. Further details on the application of the signal processing algorithm are given by Kinar and Pomeroy (2008).

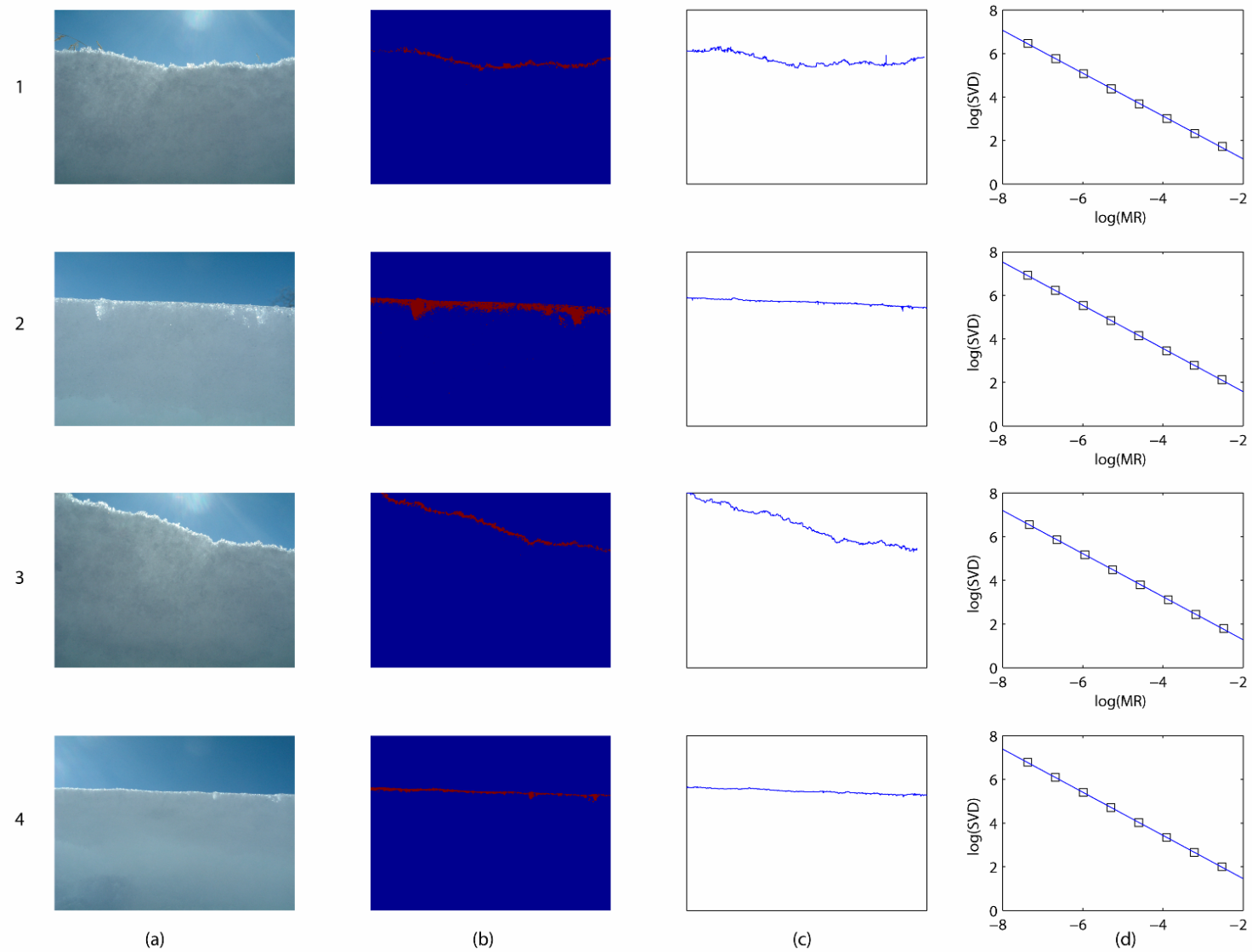

Figure 3. Determining the fractal dimension of rough snow interfaces. Four snow interfaces from a tundra site in Wolf Creek Research Basin, Whitehorse, Yukon, Canada, were analyzed (one per row). The first column (a) shows the actual image of the rough snow interface; the second column (b) shows the pixel values that are greater than a threshold value; the third column (c) shows the vertical displacement of the interface determined from the pixel values; and the fourth column (d) are the Richardson plots determined from the vertical displacements. The logarithm of the measurement resolution (MR) is plotted on the horizontal axis, whereas the logarithm of the sum of vertical displacements (SVD) is plotted on the vertical axis.

SELECTION OF PARAMETERS

Snow interfaces

An experiment was conducted to determine the fractal dimension D so that the diffuse reflection of the sound wave from the rough snow interface could be modeled. The fractal dimension was estimated from four 1600×1200 digital images taken of an actual snow interface in a windswept tundra environment. The images were taken with a Fujifilm FinePix F401 camera (Figure 3a). The images were taken from inside a snow pit during the month of April 2004 at the Wolf Creek Research Basin, Yukon, Canada. A site description of this location is given in the second paper of this series. The images taken by the digital camera were subjected to digital signal processing so that the spatial properties of the interface could be determined.

The image was converted to grayscale and the air-snow interface was determined by thresholding the pixel values. This identified the brightest pixels in the image created due to the reflection of light at the air-snow interface (Figure 3b). Spurious pixels identified by the thresholding technique were removed from the image matrix. The vertical displacement in pixels from the bottom of the image was determined by finding the maximum position of pixels which exceeded the threshold (Figure 3c). The fractal dimension D was then determined by the Richardson technique, which is widely used in image processing to characterize the fractal dimension of rough surfaces (Hamblin and Stachowiak, 1995). The Richardson technique sums the vertical displacement of the surface at increasingly coarser measurement resolutions. The logarithm of the measurement resolution (MR) is plotted on the horizontal axis of a plot, and the logarithm of the sum of vertical displacements (SVD) is plotted on the vertical axis. The slope s of the plot is determined, and the fractal dimension is calculated as $D = 1 - s$.

Figure 3d shows the Richardson plots for each of the fractal interfaces. The log-log plots are straight lines with negative slopes. This demonstrates that the snow interfaces exhibit monofractal properties because there is only one line exhibited per plot. The average fractal dimension for all

Table 1. Snow interface parameters.

Interface Number	D	R^2	Δy_{RMS}
1	1.9826	0.9998	0.4840
2	1.9906	0.9999	0.6638
3	1.9848	0.9999	0.5457
4	1.9872	0.9999	0.6034
Average	**1.9863**	**0.9999**	**0.574225**

of the four interfaces (Table1) was found to be close to a value of $D \approx 2$. This suggests that the snow interface can be modeled by fractal Brownian motion (fBm) processes (Kenkell and Walker, 1996). Due to the spectral equivalence between fBm and discrete estimators of the Weierstrass–Mandelbrot function (Molz and Liu, 1997), the results indicate that Equation (2) is likely adequate for modeling the snow interface.

The average Δy_{RMS} value was determined in units of pixels from all four images and normalized to the interval $[0,1]$. The parameters used to evaluate (2) for each interface were selected as $D = 1.9863$, $\Delta y_{RMS} = 0.574225$, $k = 1$ and $b_f = 1$.

Phase velocity

To establish the frequency range over which Equation (19) is theoretically valid, the parameters of the frequency constraint $\tilde{\omega}$ were estimated. The dynamic viscosity of air η_0 (Pa s) was calculated using Sutherland's formula (White, 1991):

$$\eta_0 = \eta_r \frac{T_r + C}{T + C}\left(\frac{T}{T_R}\right)^{3/2} \tag{23}$$

where $\eta_r = 1.827 \times 10^{-5}$ Pa·s, $T_r = 291.15$ K, $C = 120$ K are the representative values for air, and T is the ambient environmental air temperature.

For temperatures between 0 °C to –40 °C, Sutherland's formula shows that the dynamic viscosity of air ranges between $\eta_0 = 1.74 \times 10^{-5}$ kg m^{-1} s^{-1} at 0°C and $\eta_0 = 1.53 \times 10^{-5}$ kg m^{-1} s^{-1} at –40 °C. This temperature range is selected to be representative of the operating conditions for cold temperature electronics (Brown and Pomeroy, 1989). As a function of temperature and elevation, the density of air ρ_0 ranges between $\rho_0 = 0.694$ kg m^{-3} at 0°C (5000 meters above sea level) and $\rho_0 = 1.51$ kg m^{-3} at –40°C (sea level). The pore shape diameter can be estimated from (Good, 1986) as ranging between 2 mm for large-grained snow such as depth hoar and 0.1 mm for fine-grained snow. Evaluating $\tilde{\omega}$ for these ranges indicates that Equation (19) can be used within its theoretical limits for frequencies greater than ~1 Hz for large-grained snow, and for frequencies greater than ~323 Hz for fine-grained snow. These estimates could be refined with further measurements of snow geometry taken using the thin-section method (Buser and Good, 1987; Dozier *et al.*, 1987; Perla, 1985) or more recent CT-scanning methods (Kaempfer and Schneebeli, 2007; Lundy and Adams, 1998; Lundy *et al.*, 2002).

Furthermore, a high-frequency limit also applies to the P_2 wave (Nagy, 1993). To reduce excessive scattering of the incident sound wave, the wavelength λ_0 (meters) of the source must be such that $\lambda_0 > a$. Because the speed of sound in air ranges between 331 m s^{-1} at 0°C and 306 m s^{-1} at –40°C, the lowest frequency imposed is 153 kHz. Although such frequencies are limiting for the application discussed by Nagy (1993), this frequency is situated well within the ultrasonic range and far above the range of frequencies which can be produced with portable, low-power electromechanical or piezoelectric transducers. In addition, frequencies approaching 153 kHz will likely be strongly reflected at the air-snow interface. This suggests that the high-frequency limit is not applicable for the application of determining SWE by acoustic reflectometry.

Because the snowpack is a layered porous medium, other attenuation effects will also occur when the wavelength of the P_2 wave is greater than the thicknesses of the layers L_k. Due to viscous flow equilibrium in the layered porous structure, the sound pressure wave attenuation will be greatest at the relaxation frequency because the snowpack is a medium with a stiff frame. The relaxation frequency is approximated by (Pride *et al.*, 2002):

$$\omega_r \approx \frac{k_p K}{\phi y_k^2 \eta_0} \tag{24}$$

where k_p is the snow permeability (m^2), K is the bulk modulus of snow (Pa), and ϕ is the average porosity of the layers. The permeability of seasonal snow was estimated to range between $k_p = 1.83 \times 10^{-10}$ m^2 and $k_p = 8.84 \times 10^{-9}$ m^2. Representative values of the bulk modulus of snow can be obtained from (Albert, 1993a) as ranging between $K = 1.63 \times 10^6$ Pa and $K = 1.80 \times 10^7$ Pa. Because the density of seasonal snow is between 100 kg m^{-3} to 550 kg m^{-3}, snow porosities generally range between $\phi = 0.89$ to $\phi = 0.40$. Evaluating Equation (24) and assuming that the smallest thickness y_k of a layer Ω_k resolvable by the acoustic technique is in the $1 \text{ mm} \leq y_k \leq 1 \text{ m}$ range, the highest relaxation frequency is higher and lower than the critical frequency $\tilde{\omega}$. Although more precise measurements of these quantities are necessary, this estimate suggests that some measurements of SWE may not be attainable due to the strong attenuation of sound in a layered snowpack. The excessive attenuation caused due to viscous flow equilibrium of a layered snowpack would result in the negligible reflection of the sound pressure wave from the interfaces between the layers, and consequently, it would be impossible to determine SWE by the reflections of an acoustic wave.

Shape factor

Suppose that γ is unknown, and that a simplification of Equation (20) is necessary. If the porous frame is assumed to be completely rigid for snow, the induced mass could be taken as $m_I \approx 0$. In the context of Biot theory, this would also assume that the P_2 and S waves would not propagate in snow (Buckingham, 2004), although it has been postulated that shear waves may actually be produced due to interactions between the grains comprising the porous media frame (Buckingham, 2000). Returning to the derivation presented by Berryman (1980) of Equation (20), the calculated tortuosity is exactly equal to unity ($\alpha_k = 1$) when $m_I = 0$. This would imply that the boundary conditions at the air-snow and snow-snow interfaces are similar. Such an assumption is not physically reasonable and would strongly suggest that the tortuosity of snow cannot be considered as exactly equal to unity. Because empirical relationships between tortuosity and porosity have been developed for porous media (Barrande *et al.*, 2007; Dias *et al.*, 2006), the tortuosity of snow could be measured using acoustic techniques and then related to the porosity. In lieu of any experiments which have been performed to determine empirical relationships between the tortuosity and the porosity of snow, we approximate the shape factor as $\gamma = 0.59$, which is in the middle of the $0.5 \le \gamma \le 0.67$ range.

CONCLUSION

An acoustic model for the determination of SWE has been presented. In this model, the snowpack is considered to be a layered porous medium with rough interfaces. Parameters for a generated rough snow interface were selected by image analysis, which showed that these interfaces have monofractal properties. Because the fractal dimension of the interface was $D \approx 2$, this indicated that the interface could be modeled by fractal Brownian motion (fBm) processes. A version of the Weierstrass-Mandelbrot function was used to generate the snow interface, demonstrating that it is possible to generate a two-dimensional rough snow interface with fractal techniques.

A recursive relationship was used to calculate the acoustic footprint of the sound wave on the successive snow interfaces beneath the surface of the snowpack. Assuming that the sound source can be approximated as a point source, the relationship is valid for transducers situated at oblique and vertical angles of incidence. Because the surface was modeled using the V-cavity paradigm, the standard deviation of the slope angles was used to calculate the dimensionless Rayleigh parameter from wave scattering theory. The Rayleigh parameter was frequency-integrated over the bandwidth of the incident sound wave. This demonstrated that principles from sonar and radar could be applied to develop operational techniques for determining SWE.

The Berryman shape factor $\gamma = 0.59$ was taken to be a constant value. This value is in the middle of a theoretical range. Further research is required to determine if the constant value is a good choice for all sampling locations.

REFERENCES

Albert DG. 1987. The effect of snow on vehicle-generated seismic signatures. *Journal of the Acoustical Society of America* **81**(4): 881-887.

Albert DG. 1993a. *Attenuation of outdoor sound propagation levels by a snow cover, CRREL Report 93-20*. Cold Regions Research and Engineering Laboratory: Hanover, New Hampshire.

Albert DG. 1993b. A comparison between wave propagation in water-saturated and air-saturated porous materials. *Journal of Applied Physics* **73**(1): 28-36.

Albert DG. 2001. Acoustic waveform inversion with application to seasonal snow covers. *Journal of the Acoustical Society of America* **109**(1): 91-101.

Albert DG, Orcutt JA. 1989. Observations of low-frequency acoustic-to-seismic coupling in the summer and the winter. *Journal of the Acoustical Society of America* **86**(1): 352-359.

Albert DG, Orcutt JA. 1990. Acoustic pulse propagation above grassland and snow: comparison of theoretical and experimental waveforms. *Journal of the Acoustical Society of America* **67**(1): 93-100.

Alberverio S, Pratsiovytyi M, Torbin G. 2004. Fractal probability distributions and transformations preserving the Hausdorff–Besicovitch dimension. *Ergodic Theory and Dynamical Systems* **24**: 1-16.

Arcone SA, Yankielun NE, Edward F. Chacho J. 1997. Reflection Profiling of Arctic Lake Ice Using Microwave FM-CW Radar. *IEEE Transactions on Geoscience and Remote Sensing* **35**(2): 436-443.

Barrande M, Bouchet R, Denoyel R. 2007. Tortuosity of porous particles. *Analytical Chemistry* **79**(23): 9115-9121.

Berryman JG. 1980. Confirmation of Biot's theory. *Applied Physics Letters* **37**(4): 382-384.

Berryman JG. 1983. Effective conductivity by fluid analogy for a porous insulator filled with a conductor. *Physical Review B* **27**(12): 7789-7792.

Biot MA. 1956a. Theory of propagation of elastic waves in a fluid-saturated porous solid I. Low Frequency Range. *Journal of the Acoustical Society of America* **28**(2): 168-178.

Biot MA. 1956b. Theory of propagation of elastic waves in a fluid-saturated porous solid. II. Higher frequency range. *Journal of the Acoustical Society of America* **28**(2): 179-191.

Borish J, Angell JB. 1983. An efficient algorithm for measuring the impulse response using pseudorandom noise. *Journal of the Audio Engineering Society* **31**(7): 478-487.

Brekhovskikh LM, Lysanov YP. 2003. *Fundamentals of Ocean Acoustics, 3rd Edition*. Springer-Verlag: New York.

Brown T, Pomeroy JW. 1989. A blowing snow detection gauge. *Cold Regions Science and Technology*: 167-174.

Buckingham MJ. 2000. Wave propagation, stress relaxation, and grain-to-grain shearing in saturated, unconsolidated marine sediments. *Journal of the Acoustical Society of America* **108**: 2796-2815.

Buckingham MJ. 2004. A three-parameter dispersion relationship for Biot's fast compressional wave in a marine sediment. *Journal of the Acoustical Society of America* **116**(2): 769-776.

Buser O, Good W. 1987. Acoustic, geometric and mechanical parameters of snow. *Avalanche Formation, Movement and Effects, Proceedings of the Davos Symposium*: 61-71.

Cai Z, Chen D, Lu S. 2006. Reconstruction of a fractal rough surface. *Physica D: Nonlinear Phenomena* **213**(1): 25-30.

Claps P, Fiorentino M, Oliveto G. 1996. Informational entropy of fractal river networks. *Journal of Hydrology* **187**(1-2): 145-156.

Coléou C, Lesaffre B, Brzoska JB, Ludwig W, Boller E. 2001. Three-dimensional snow images by X-ray microtomography. *Annals of Glaciology* **32**: 75-81.

Dias R, Teixeira JA, Mota M, Yelshin A. 2006. Tortuosity variation in a low density binary particulate bed. *Separation and Purification Technology* **51**(2): 180-184.

Dozier J, Davis RE, Perla R. 1987. On the objective analysis of snow microstructure. *Avalanche Formation, Movement and Effects, Proceedings of the Davos Symposium*: 49-58.

Falconer K. 1990. *Fractal geometry : mathematical foundations and applications*. Wiley: Chichester; New York.

Good W. 1986. Thin sections, serial cuts and 3-D analysis of snow. *Avalanche Formation, Movement and Effects, Proceedings of the Davos Symposium*: 35-48.

Hamblin MG, Stachowiak GW. 1995. Application of the Richardson technique to the analysis of surface profiles and particle boundaries. *Tribology Letters* **1**: 95-108.

Johnson DL, Plona TJ. 1982. Acoustic slow waves and the consolidation transition. *Journal of the Acoustical Society of America* **72**(2): 556-565.

Johnson DL, Scala C, Pasierb F, Kojima H. 1982. Tortuosity and acoustic slow waves. *Physical Review Letters* **49**(25): 1840-1844.

Johnson DL, Sen PN. 1981. Multiple scattering of acoustic waves with application to index of refraction of fourth sound. *Physical Review B* **24**(5): 2486-2496.

Johnson JB. 1982. On the application of Biot's theory to acoustic wave propagation in snow. *Cold Regions Science and Technology* **6**: 49-60.

Jones HG, Pomeroy JW, Davies TD, Tranter M, Marsh P. 1999. CO2 in Arctic snow cover: landscape form, in-pack gas concentration gradients, and the implications for the estimation of gaseous fluxes. *Hydrological Processes* **13**(18): 2977 - 2989.

Kaempfer TU, Schneebeli M. 2007. Observation of isothermal metamorphism of new snow and interpretation as a sintering process. *Journal of Geophysical Research* **112**(D24101):

Kaempfer TU, Schneebeli M, Sokratov SA. 2005. A microstructural approach to model heat transfer in snow. *Geophysical Research Letters* **32**: L21503.

Kenkell NC, Walker DJ. 1996. Fractals in the Biological Sciences. *Coenoses* **11**(2): 77-100.

Kerbrat M, Pinzer B, Huthwelker T, Gaggeler HW, Ammann M, Schneebel M. 2008. Measuring the specific surface area of snow with X-ray tomography and gas adsorption: comparison and implications for surface smoothness. *Atmospheric Chemistry and Physics* **8**: 1261–1275.

Kinar NJ, Pomeroy JW. 2007. Determining snow water equivalent by acoustic sounding. *Hydrological Processes* **21**: 2623-2640.

Kinar NJ, Pomeroy JW. 2008. Automated determination of Snow Water Equivalent by acoustic reflectometry. *IEEE Journal of Geoscience and Remote Sensing*: submitted.

Lapidus M, Pang M. 1995. Eigenfunctions of the Koch snowflake domain *Communications in Mathematical Physics* **172**(2): 359-376.

Lundy C, Adams EE. 1998. Non-destructive collection of natural snow samples for use with CT scan analysis. *Proceedings of the International Snow Science Workshop* **11**: n.p.

Lundy CC, Edens MQ, Brown RL. 2002. Measurement of snow density and microstructure using computed microtomography. *Journal of Glaciology* **48**(161): 312-316.

Lurton X. 2002. *An introduction to underwater acoustics : principles and applications*. Springer; Praxis Publishing: New York; Chichester, UK.

Molz FJ, Liu HH. 1997. Fractional Brownian motion and fractional Gaussian noise in subsurface hydrology: a review, presentation of fundamental properties, and extensions. *Water Resources Research* **33**(10): 2273-2286.

Nagy PB. 1993. Slow wave propagation in air-filled permeable solids. *Journal of the Acoustical Society of America* **93**(6): 3224-3234.

Perla R. 1985. Snow in strong or weak temperature gradients. Part II: Section-plane analysis. *Cold Regions Science and Technology* **11**: 181-186.

Pomeroy JW, Gray DM. 1995. *Snowcover accumulation, relocation, and management, National Hydrology Research Institute Science Report No. 7*. National Water Research Institute: Saskatoon, Canada.

Pomeroy JW, Gray DM, Brown T, Hedstrom NR, Quinton WL, Granger RJ, Carey SK. 2007. The cold regions hydrological model: a platform for basing process representation and model structure on physical evidence. *Hydrological Processes* **21**: 2650–2667.

Pomeroy JW, Schmidt RA. 1993. The Use of Fractal Geometry in Modelling Intercepted Snow Accumulation and Sublimation. *Proceedings of the Eastern Snow Conference* **50**: 1-10.

Pride SR, Tromeur E, Berryman JG. 2002. Biot slow-wave effects in stratified rock. *Geophysics* **67**(1): 271-281.

Rife DD, Vanderkooy J. 1989. Transfer-function measurement with maximum-length sequences. *Journal of the Audio Engineering Society* **37**(6): 419-444.

Shishikura M. 1998. The Hausdorff Dimension of the Boundary of the Mandelbrot Set and Julia Sets. *The Annals of Mathematics* **147**(2): 225-267.

Shook K, Gray DM. 1997. Synthesizing shallow seasonal snow covers. *Water Resources Research* **33**(3): 419-426.

Shook K, Gray DM, Pomeroy JW. 1993. Temporal variation in snowcover area during melt in Prairie and Alpine environments. *Nordic Hydrology*: 183-198.

Sornette D. 2006. *Critical Phenomena in Natural Sciences* Springer Berlin Heidelberg: Berlin.

Suman R, Ruth D. 1993. Formation factor and tortuosity of homogeneous porous media. *Transport in Porous Media* **12**: 185-206.

Summers JE, Soukup RJ, Gragg RF. 2005. *Characterization and Fabrication of Synthetic Rough Surfaces for Acoustical Scale-Model Experiments, Naval Research Laboratory Report NRL/MR-MM/7140--05-8871*. Naval Research Laboratory: Washington, D.C.

Szulga J. 2002. Hausdorff dimension ofWeierstrass–Mandelbrot process. *Statistics & Probability Letters* **56**: 301–307.

Torrance K, Sparrow E. 1967. Theory for Off-Specular Reflection from Rough Surfaces. *Journal of the Optical Society of America* **57**(9): 1105-1112.
Tyre AJ, Possingham HP, Lindenmayer DB. 1998. Modelling dispersal behaviour on a fractal landscape. *Environmental Modelling and Software* **14**(1): 103-113.
Vogel HJ, Roth K. 2003. Moving through scales of flow and transport in soil. *Journal of Hydrology* **272**(1-4): 95-106.
Wang R, Pavlin T, Rosen MS, Mair RW, Cory DG, Walsworth RL. 2005. Xenon NMR measurements of permeability and tortuosity in reservoir rocks. *Magnetic Resonance Imaging* **23**(2): 329-331.
White FM. 1991. *Viscous fluid flow*. McGraw-Hill Higher Education: New York.